ACS APPLIED MATERIALS & INTERFACES
Letter
www.acsami.org

Anisotropic Adhesion of Micropillars with Spatula Pads

Seungwan Seo,[†] Jehong Lee,[†] Kwang-Seop Kim,[‡] Kwang Hee Ko,[†] Jong Hyun Lee,[†] and Jongho Lee*[,†]

[†]Gwangju Institute of Science and Technology (GIST), Mechatronics, 123 Cheomdan-gwagiro, Buk-gu, Gwangju 500-712, Republic of Korea

[‡]Nano-Convergence Mechanical Systems Research Division, Korea Institute of Machinery & Materials (KIMM), 156 Gajungbukno, Yuseong-gu, Daejeon 305-343, Republic of Korea

S Supporting Information

ABSTRACT: Natural gecko adhesive structures consisting of angled setae, branched into thin spatulas, have remarkable properties including easily attachable and releasable anisotropic adhesion. The geometrically asymmetric structures lead to anisotropic adhesive properties. Inspired by the gecko, we fabricated an array of micropillars with asymmetric spatula pads from elastomeric materials. This paper describes the anisotropic properties of the micropillars with spatula pads as established by experimental measurements and observation together with finite element analysis. The results indicate that the structural difference of the spatula pad at one edge of the micropillar provides the anisotropic adhesive properties.

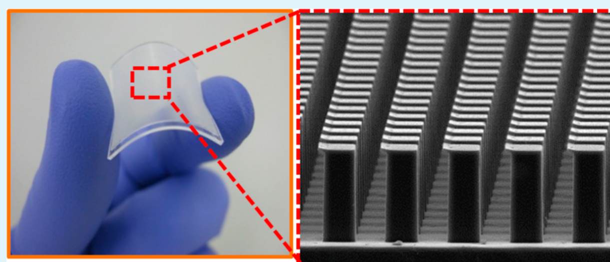

KEYWORDS: *gecko, spatula, adhesive, adhesion, biomimetics, bio-inspiration*

■ INTRODUCTION

Recent research in experimental biology and mechanics has examined the unique properties of natural gecko adhesives, including easy attach, easy release, self-cleaning, and many others.[1−3] These properties enable geckos to quickly climb walls and walk upside down on ceilings while keeping their adhesive feet clean enough to hold their body weight in most environments, including their natural habitat and human houses.[4,5] Those features have inspired engineers to develop gecko-type adhesives for diverse applications that require easily releasable adhesives, including household or medical tapes, sporting goods, wall climbing robots, semiconductor carriers, and many others.[6−12] The approaches vary depending on fabrication methods, desired properties or targeted applications, and current structural designs include vertical, angled, or hierarchical pillars using diverse materials such as polymers, carbon nanotubes, inorganic nanowires, or composites of these materials.[13−27]

One structural design parameter involves the use of angled micropillars, which can produce strong directional adhesion.[7,9,10,28] Such micropillars mimic the natural hierarchical fibrillar setae structures found on gecko feet, and typically have thin and wide endings, or spatulas, at the tip, which branch from the long slender setae. The thin spatulas maximize contact area while the long slender setae provide compliance, i.e., a lower effective modulus,[29] satisfying Dahlquist's criterion for tack. Importantly, changing the design of the micropillars' endings affects their adhesion properties. For example, studies have shown that mushroom-shaped micropillars with thin wide flaps at the end provide higher than normal adhesion.[30−33] Micropillars with triangular-shaped tips have exhibited anisotropic adhesive properties resulting from cracks on the triangular vertex or triangular sides.[34] These mushroom-shaped and triangular-tip-shaped micropillars terminate in thin and wide flaps that encircle the end of the micropillars. Micropillars tipped with asymmetric spatula-like terminals also provide higher than normal adhesion.[31,32] And, thin flaps protruding from only one side of the micropillars, similar to the gecko's spatula, will provide anisotropic adhesion that is determined by the thin flaps' location. Hereafter, we call these thin flaps spatula pads.

Here, we report the anisotropic properties of micropillars with spatula pads that were fabricated with conventional semiconductor processing technology. We describe methods for fabricating the mold used for casting and curing the elastomeric micropillars with spatula pads. Experimental measurements and finite element modeling were used to investigate the anisotropic properties of the fabricated micropillars, such as the adhesive forces at retraction and their dependence on retraction angles and direction. The one-directional spatula pads produced effects that prevented delamination from starting at the edge of the micropillar, resulting in higher adhesion when retraction was opposite to the direction of the spatula pads.

■ RESULTS AND DISCUSSION

The process for fabricating the array of micropillars with spatula pads appears in Figure 1. We first made deep holes, followed by the fabrication of shallow steps in silicon wafer using deep reactive ion etching (DRIE) with masks of photoresist and SiO_2, respectively, as shown in Figure 1a. Applying voltage (∼ 900 V

Received: October 7, 2013
Accepted: January 21, 2014
Published: January 21, 2014

© 2014 American Chemical Society

dx.doi.org/10.1021/am4044135 | *ACS Appl. Mater. Interfaces* 2014, 6, 1345−1350

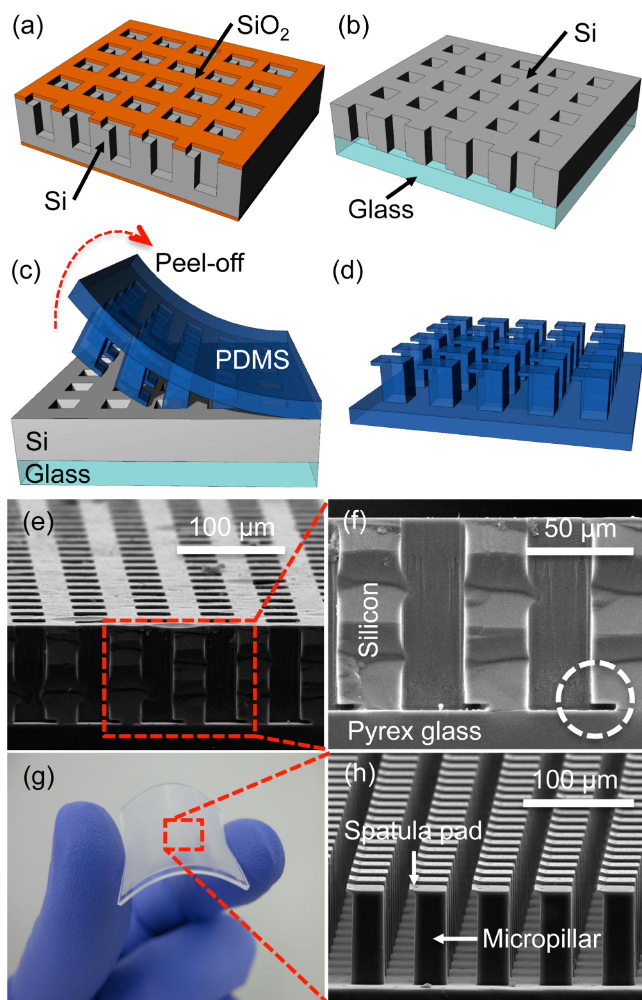

Figure 1. Schematic illustration of the fabrication process, and scanning electron microscopy (SEM) and optical images of micropillars with spatula pads. (a) In the first step of the fabrication, sequential deep reactive ion etching (DRIE) of a silicon wafer with masks of photoresist and SiO_2 makes deep holes (size ∼30 μm × 30 μm, depth ∼90 μm) and shallow steps (size ∼12 μm × 30 μm, depth ∼3 μm), respectively. Period of the square holes is 60 μm. (b) Anodic bonding process firmly bonds the silicon wafer, with the shallow steps facing down, to Pyrex glass. Opening the deep holes by removing the backing of the silicon wafer through another DRIE process completes the fabrication process of a master mold. (c) The casting and curing process of polydimethylsiloxane (PDMS) into the master mold makes replicas of (d) micropillars with the spatula pads. (e, f) SEM cross-sectional images of the completed master mold. (f) The SEM image clearly shows the flat spaces for spatula pads, noted by a dashed circle. (g) Optical image of the replica micropillar array. (size ∼2 cm ×2 cm) (h) SEM image of the completed micropillars with spatula pads.

with a current of 40 mA) at raised temperature (∼350 °C) and pressure (∼5 N/cm^2), we stably bonded the silicon mold, with holes facing down, onto Pyrex glass. Opening the deep holes by etching away the backing with another DRIE process completed the fabrication process for the master mold as shown in Figure 1b. Polydimethylsiloxane (PDMS) was cast into the master mold, then cured and peeled away, creating a simple means to produce elastomeric replicas of the micropillars with spatula pads, as shown in panels c and d in Figure 1. Peeling the replicas starting from the side opposite the spatula pads prevented the thin spatula pads from tearing off. See the Experimental Section and Figure S1 in the Supporting Information for further details.

Figure 1e is a scanning electron microscopy (SEM) image of a cross-section of the completed master mold, which consists of deep square holes with edge lengths of 30 μm and depths of 90 μm. The center-to-center distance of the square holes is 60 μm. Each square hole has one shallow space of ∼12 μm × 30 μm, with thickness ∼3 μm protruding horizontally to one edge at the bottom, as shown in the magnified image of Figure 1f. The magnified image also confirms the solid bonding between the structured silicon wafer and Pyrex glass. Degassing for 3 h was sufficient to allow the deep squares holes and shallow spaces to be filled with a mixture of silicone elastomer base and cross-linking agent. The PDMS mixture was then cured at 70 °C for 2 h. This fabrication technology can be scaled up to any size of silicon wafer, however, we confined the size of the master mold, and thus, the array of micropillars with spatula pads to 2 × 2 cm^2 as shown in Figure 1g. The SEM image of Figure 1h clearly shows the micropillars with spatula pads. Each elastomeric micropillar has a thin spatula pad with a thickness of 3 μm, protruding 12 μm horizontally out of one edge of the micropillar tip.

This asymmetric structure, with spatula pads overhanging one edge, provides anisotropic adhesive characteristics that depend on the angle at which the pad is detached. To examine the detailed performance of the micropillars with spatula pads, we built a measurement apparatus consisting of a multi-axis force sensor and multi-axis microstage. The microstage could be programmed to move through a predefined path, while the bottom of the micropillars were observed through a glass substrate with a microscope mounted on top, as shown in Figure 2a. See the Experimental Section for further details on the measurement apparatus.

Figure 2b illustrates the methods used for measuring anistropic adhesive characteristics upon detachment. The array of micropillars with spatula pads (∼7 × 7 mm^2), mounted on the force sensor, approaches a flat transparent glass substrate, makes contact, and then retracts from the substrate at an angle either along (θ_{along}) or against ($\theta_{against}$) the orientation of the spatula pad. In other words, retraction in the direction that is opposite to the orientation of the spatula pad is called "along" with the angle θ_{along}. In contrast, retraction in the same direction as the spatula pad orientation is denoted as "against" with the angle $\theta_{against}$. Careful alignment was used to ensure the planar body of the micropillar array was maintained parallel to the glass substrate when approaching vertically to the substrate, and when retracting at an angle of θ_{along} or $\theta_{against}$ away from the substrate. A flat glass substrate was used to avoid any effects on measurement caused by a spherical substrate.[35] We used a dual-axis tilting stage to ensure the micropillars all contacted the flat substrate simultaneously. See the Experimental Section for further details. We programmed the micropillar array's vertical approach to the flat glass substrate to be relatively slow (∼20 μm/s) to avoid overshooting, until the compressive force, i.e., preload, reached 2 N. Then the micropillar array was retracted at an angle of θ_{along} or $\theta_{against}$ from the substrate at 200 μm/s. The retraction speed was high enough to ensure that the micropillars detached simultaneously, because at a lower retraction speed many of them would detach individually, even though the geometry of the micropillars was uniform.[36] See Figure S2 in the Supporting Information for effects of the preload and retraction speed.

The measurement results, as shown in Figure 3, describe the anisotropic adhesive characteristics of the micropillar array with spatula pads according to the retracting direction. Figure 3a and 3b present the normal and shear forces measured when the micropillar array vertically approached and retracted from the

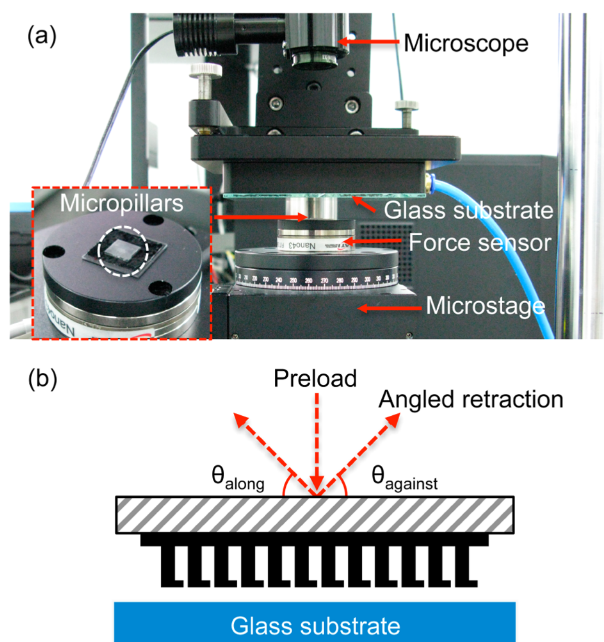

Figure 2. Experiment set-up and measurement methods for the micropillars with spatula pads. (a) Optical image of the experimental setup to characterize adhesion properties of the micropillar array. The custom-built experimental setup consists of multi-axis force sensors and programmable motorized microstages to characterize adhesive forces on a smooth glass substrate while monitoring the micropillars with an optical microscope mounted on top. (b) Schematic illustration of the measurement method. The micropillar array approaches a glass substrate vertically. Once the normal load reaches a preload of 2 N, the micropillar array retracts with an angle, θ_{along} or $\theta_{against}$ from the glass substrate.

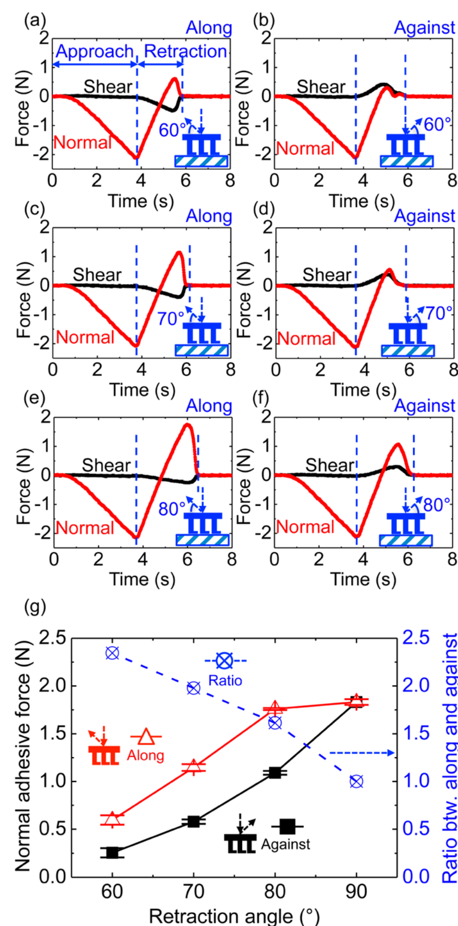

Figure 3. Measurement results of the micropillars with spatula pads depending on retraction direction and angle. (a, b) Characteristics of normal and shear forces of the micropillars when retracting at 60° (a) along and (b) against the spatula pads. Compressive normal force reaches 2 N without changes in shear force when the array of micropillars approaches the glass substrate vertically. During retraction along the spatula pads at 60°, normal force changes to adhesive force with a peak of 0.25 N. For the same experiment against the spatula pads, the maximum normal adhesive force is 0.59 N. (c−f) Normal and shear forces of the micropillars when retracting at (c, d) 70 and (e, f) 80°. Normal adhesive forces are (c) 0.57 and (d) 1.14 N, and (e) 1.09 and (f) 1.75 N, respectively, when retracting along or against the spatula pads at 70 and 80°. Normal forces, along the spatula pads, are larger than forces when retracting against spatula pads. (g) Ratio of normal adhesives forces of the micropillar array at detachment when retracting with angles of θ_{along} and $\theta_{against}$. The measurement was repeated 20 times at each retraction angle. The normal adhesive forces are 2.3, 2.0, and 1.6 times higher at the angle of 60, 70, and 80°, respectively, when retracting through θ_{along} than for $\theta_{against}$, although adhesive force increases at higher retraction angle.

glass substrate along and against the spatula pads at 60°. At lower retraction angles (< 50°), including dragging the spatula pads horizontally, the thin soft spatula pads exhibit an extra effect, overturning in the region of compressive normal force because of shearing. See Figure S3 in the Supporting Information for details. When approaching vertically, the normal force, plotted in red, is compressive, negative and turns to tensile, positive, during angled retraction. The sign of shear resistance, plotted in black, depends on the direction of retraction. The normal adhesive force (∼0.59 N) along the spatula pads is 2.3 times higher than the force (∼0.25 N) against the spatula pads. Shear resistances for along and against are 0.50 and 0.41 N, respectively.

When retracting at a higher angle of 70°, as in Figure 3c, d, and 80°, as in Figure 3e, f, normal adhesive forces along the spatula pads are larger than those against the spatula pads at each angle; however, they increase as much as 1.14 N and 0.57 N for 70° and as much as 1.75 N and 1.09 N for 80°, respectively. These results indicate that the asymmetric geometry of the spatula pads provides anisotropic effects in adhesion. The adhesive force at normal retraction, i.e., an angle of 90° is 1.83 N. Figure 3g shows the ratio of normal adhesive forces at retraction for along and against. We repeated the measurement 20 times at each angle. Although the normal adhesive force is larger at a higher retraction angle, the ratio of normal adhesive forces is relatively lower at higher retraction angle. The ratios of the normal adhesive forces are 2.3, 2.0, and 1.6 for 60, 70, and 80°, respectively.

The adhesive forces per unit area of the micropillars with spatula pads (normal, 5.1−37.3 kPa; shear, 2.2−10.2 kPa; normal/shear, 1.2−16.7) were relatively low compared with a gecko's natural setal array, which consists of hierarchical nano and microstructures (normal, 48 kPa; shear, 184 kPa; normal/shear, 0.26).[1,4,37] Although the determination of adhesive forces depends on the measurement methods, e.g., flat or spherical contact surfaces, the normal adhesive forces reported for mushroom-shaped micropillars are relatively higher than those reported here, because the thin and wide flaps completely surround the micropillar tips (normal, 180 kPa;[30] normal, 60.6 kPa[33]), see Table S1 in the Supporting Information.

Here, the anisotropic adhesive characteristics are attributed to the thin spatula pads extending from the bottom of the micropillars horizontally through a single side of their edges.

Figure 4a−c shows the bottom view, side view, and finite element method (FEM) model, respectively, of the micropillars in contact with the glass substrate in neutral state, i.e., without shearing. In this condition, micropillars and spatula pads are in contact with the glass substrate. With a slight shearing of the array, by about 12 μm, delamination starts from around the area where the micropillars and spatula pads intersect, which are the dark regions noted with the dashed squares in Figure 4d. The side view of the micropillar in Figure 4e clearly shows delamination at the bottom of the micropillar, while the tip of the spatula pad is still in contact with the glass substrate. The FEM model, with an assumption of a fixed boundary at the bottom, indicates that the maximum tensile stress occurs around the intersection of the micropillar and spatula pad, noted by a dashed arrow in Figure 4f. The place of maximum tensile stress from the FEM analysis matches well with the delamination observed experimentally. See Figure S4 in the Supporting Information for the geometric parameters in the FEM analysis. The experimental observation and FEM model indicate that the concentrated tensile stress initiates delamination around the intersection while the other regions remain in contact. In contrast, panels g and h in Figure 4 show delamination starting from the heel of the micropillar, the side opposite the spatula pad, when the top of the micropillar is displaced horizontally. The FEM model in Figure 4i, indicating the maximum tensile stress around the heel of the micropillar, matches well with the experimental observation.

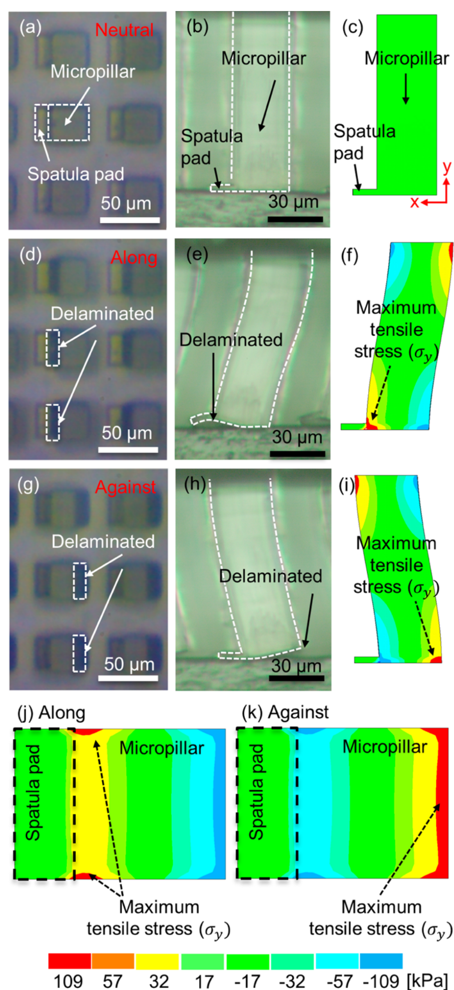

Figure 4. Optical microscope images and finite element method (FEM) results of the micropillars in contact with an optically transparent glass substrate. (a) Bottom and (b) side view of the micropillars with spatula pads preloaded vertically onto a glass substrate. The images indicate that the (a) bottoms of the micropillar and spatula pad are in contact with a glass substrate and (b) the micropillar is straight up in the neutral posture. (c) FEM results of the micropillar with spatula pads in neutral state without any shearing. (d) Bottom and (e) side view of the micropillars sheared slightly along the spatula pads. The dark area indicated by the dashed rectangles shows a delaminated region. The images clearly indicate that delamination starts from the bottom between the spatula pad and micropillar. The spatula pads are still in contact even after the delamination starts. (f) FEM result for the tensile stress of the micropillars whose bottoms are fixed and tops are displaced by 12 μm along the spatula pad. The dashed arrows indicate the places of maximum tensile stress in the micropillars. The point where the maximum tensile stress occurs in the FEM results agrees with the points where delamination starts as observed experimentally. (g, h) Image of the micropillars sheared against the spatula pads. Delamination that starts from the heel of the micropillars provides a better chance to propagate, resulting in lower adhesion. (i) The FEM result also indicates where the maximum tensile stress occurs in the micropillars when the top of the micropillars are displaced by 12 μm from the spatula pad. The point of maximum tensile stress, i.e., the heel of the micropillar, also agrees well with the experimental results. (j, k) FEM results for the bottom surface of the micropillar when the top of the micropillar is displaced by 12 μm (j) along and (k) against the spatula pad.

In addition to the difference in where delamination starts, there is a difference in the location of maximum tensile stress depending on the shearing direction. The maximum tensile stress around the heel when shearing against the spatula pads (∼109 kPa), as in Figure 4i, is 1.15 times higher than the maximum tensile stress around the spatula pads (∼94 kPa) when shearing is along, as in Figure 4f. This reduction in maximum tensile stress at the interface is attributed to the relief of concentrated stress due to the presence of the spatula pad. Panels j and k in Figure 4 show the distribution of normal stress at the bottom surface of the micropillar with spatula pad when the top of the micropillar is displaced by 12 μm. As shown in Figure 4j, the tensile stress is more uniformly distributed over the spatula pad, resulting in reduced maximum tensile stress compared to the tensile stress around the heel of the micropillar when displaced in the other direction, as shown in Figure 4k. The FEM model also indicates that shear resistance depends on the aspect ratio of the micropillars. Low aspect ratio micropillars induce less tensile stress, as shown in Figure S5 in the Supporting Information.

CONCLUSION

Simple design parameters were used to fabricate micropillars having spatula pads protruding asymmetrically at the tip, which exhibited anisotropic properties based on the external manipulation of the array, such as the variation of retraction direction or angles. Further optimizing and adjusting of the size of the micropillars and spatula pads, in addition to changing the materials to have different mechanical properties, should lead to further improvement in these anisotropic properties.

EXPERIMENTAL SECTION

Fabricating the Master Mold for Micropillars with Spaula Pads. We started the fabrication process by photolithographically patterning a silicon dioxide (SiO_2) layer, (thickness ∼300 nm) thermally formed on a double side polished silicon wafer (thickness ∼200 μm). Reactive ion etching (RIE) process removed the exposed thermal silicon dioxide layer, forming hard mask patterns of SiO_2 on Si wafer. The defined patterns of the

thermal oxide layer provided a hard mask for the merged area (~42 μm × 30 μm) of the micropillars (size ~30 μm × 30 μm) and spatula pads (size ~12 μm × 30 μm). A second lithography with relatively thick photoresist (thickness ~7 μm) made openings only for the micropillars (size ~30 μm × 30 μm). Deep reactive ion etching (DRIE, Alcatel AMS200) was used to make an array of square holes (size ~30 μm × 30 μm, depth ~90 μm, period ~60 μm). After ashing of the residual photoresist, another DRIE process formed shallow steps (size ~12 μm × 30 μm, depth ~3 μm) for spatula pads through the hard mask of thermal SiO_2 layer. Each deep hole for a micropillar had an attached shallow step for a spatula pad. We bonded the Si wafers, with the pattered surface facing down, to Pyrex glass, through standard anodic bonding process (temperature ~350°C, pressure ~0.5 kgf/cm^2, voltage ~900 V with a current of 40 mA) after depositing a thermal SiO_2 layer to protect the structures in the subsequent etching process. We finally removed the backside of the Si wafers through DRIE without any mask to reach the bottom of the deep holes. Cleaning the master mold with hydrofluoric acid (HF) completed the process. See Figure S1 in the Supporting Information for details.

Forming PDMS Replicas of Micropillars with Spatula Pads. Casting and curing methods[38] were used to make replicas of micropillars with spatula pads with the master mold. A mixture of silicone elastomer base and cross-linking agent at a ratio of 10:1 (Sylgard 184, Dow corning) was poured into the master mold after silane (Sigma Aldrich) treatment for 2 h. Degassing in vacuum for 3 h removed air bubbles trapped in the shallow space for the spatula pads. We controlled the thickness of the backing layer of the replicas with a hydrophobic glass plate fixed to an external post whose height was manually adjustable. We cured the PDMS mixture in the mold at 70°C for 2 h. Peeling off the cured replica carefully from the side opposite the spatula pads completed the fabrication process.

Building up the Measurement Apparatus. The performance of the micropillars with spatula tips was characterized with a custom-built measurement apparatus that consists of a multi-axis force sensor, (ATI Industrial Automation) multi-axis microstage, (Cheungwon Electronics) and microscope.(Olympus) The programmable microstage mounting an array of micropillars is capable of moving to the desired location at a desired speed while monitoring adhesive forces through a data acquisition board (NI instrument) in real-time. We aligned the glass substrate mounted on a dual axis tilting stage to the array of micropillars by visually inspecting the contact regions between the micropillars and glass substrate through the microscope.

Measuring the Adhesive Characteristics. We mounted an array of the micropillars with the spatula pads (size of the array ~7 × 7 mm^2) onto the force sensor equipped on the microstage. The glass substrate was aligned parallel to the array of micropillars using the dual-axis tilting stage so that the micropillars made contact with the glass substrate almost at the same time when the array on the microstage approached the substrate. We also aligned one of the horizontal axes of the force sensor to the axis of horizontal movement of the microstage using a rotational stage to avoid off-axis errors. We cleaned the samples with isopropyl alcohol (IPA) ahead of each experiment. The microstage mounting the micropillar array was programmed to approach the glass substrate normally until a normal preload reached about 2 N. After reaching the desired preload, the micropillars with spatula pads were retracted at desired angles along or against the spatula pads at a constant speed (~200 μm/s). We monitored adhesive forces in real time and collected the data with the multi-axis force sensor through a data acquisition card with a sampling rate of 100 Hz. We repeated the measurement 20 times along and against the spatula pads for each angle.

■ ASSOCIATED CONTENT

S Supporting Information

Illustrations of the fabrication process, overturning effects of spatula pads, effects of retraction speeds and preloads, geometric parameters and meshed elements for the FEM model, and FEM results of the micropillars at the bottom surface. This material is available free of charge via the Internet at http://pubs.acs.org.

■ AUTHOR INFORMATION

Corresponding Author

*E-mail: jong@gist.ac.kr.

Notes

The authors declare no competing financial interest.

■ ACKNOWLEDGMENTS

This work was supported by the National Research Foundation of Korea (NRF) grant funded by the Korea government (MSIP) (2013R1A1A1007512, 2013M1A3A3A02042560) and by the Development Program of Manufacturing Technology for Flexible Electronics with High Performance (SC0970) funded by the Korea Institute of Machinery and Materials.

■ REFERENCES

(1) Autumn, K.; Liang, Y. A.; Hsieh, S. T.; Zesch, W.; Chan, W. P.; Kenny, T. W.; Fearing, R.; Full, R. J. *Nature* **2000**, *405*, 681−685.
(2) Autumn, K. *MRS Bull.* **2007**, *32*, 473−478.
(3) Autumn, K. Properties, Principles, and Parameters of the Gecko Adhesive System. In *Biological Adhesives*; Smith, A. M., Callow, J. A., Eds.; Springer: Berlin, 2006; pp 225−255.
(4) Autumn, K.; Dittmore, A.; Santos, D.; Spenko, M.; Cutkosky, M. *J. Exp. Biol.* **2006**, *209*, 3569−3579.
(5) Hansen, W. R.; Autumn, K. *Proc. Natl. Acad. Sci. U.S.A.* **2005**, *102*, 385−389.
(6) Crosby, A. J.; Hageman, M.; Duncan, A. *Langmuir* **2005**, *21*, 11738−11743.
(7) Kim, S.; Spenko, M.; Trujillo, S.; Heyneman, B.; Santos, D.; Cutkosky, M.R. *IEEE Trans. Rob.* **2008**, *24*, 65−74.
(8) Parness, A.; Soto, D.; Esparza, N.; Gravish, N.; Wilkinson, M.; Autumn, K.; Cutkosky, M. *J. R. Soc., Interface* **2009**, *6*, 1223−1232.
(9) Lee, J.; Fearing, R. S.; Komvopoulos, K. *Appl. Phys. Lett.* **2008**, *93*, 191910.
(10) Kim, T.-I.; Jeong, H. E.; Suh, K. Y.; Lee, H. H. *Adv. Mater.* **2009**, *21*, 2276−2281.
(11) Moon, M.-W.; Cha, T.-G.; Lee, K.-Y.; Vaziri, A.; Kim, H.-Y. *Soft Matter* **2010**, *6*, 3924−3929.
(12) Northen, M. T.; Turner, K. L. *Sens. Actuators, A* **2006**, *130*, 583−587.
(13) Greiner, C.; Artz, E.; del Campo, A. *Adv. Mater.* **2009**, *21*, 479−482.
(14) Murphy, M. P.; Kim, S.; Sitti, M. *ACS Appl. Mater. Interfaces* **2009**, *1*, 849−855.
(15) Lee, J.; Majidi, C.; Schubert, B.; Fearing, R. S. *J. R. Soc., Interface* **2008**, *5*, 835−844.
(16) Kim, S.; Sitti, M.; Xie, T.; Xiao, X. *Soft Matter* **2009**, *5*, 3689−3693.
(17) Sitti, M.; Cusick, B.; Aksak, B.; Nese, A.; Lee, H.; Dong, H.; Kowalewski, T.; Matyjaszewski, K. *ACS Appl. Mater. Interfaces* **2009**, *1*, 2277−2287.
(18) Ko, H.; Lee, J.; Schubert, B. E.; Chueh, Y.-L.; Leu, P. W.; Fearing, R. S.; Javey, A. *Nano Lett.* **2009**, *9*, 2054−2058.

(19) Shen, L.; Glassmaker, N. J.; Jagota, A.; Hui, C.-Y. *Soft Matter* **2008**, *4*, 618−625.
(20) Bae, W.-G.; Kwak, M. K.; Jeong, H. E.; Pang, C.; Jeong, H.; Suh, K. Y. *Soft Matter* **2013**, *9*, 1422−1427.
(21) Qu, L.; Dai, L.; Stone, M.; Xia, Z.; Wang, Z. L. *Science* **2008**, *322*, 238−242.
(22) Hu, S.; Jiang, H.; Xia, Z.; Gao, X. *ACS Appl. Mater. Interfaces* **2010**, *2*, 2570−2578.
(23) Jeong, H. E.; Lee, J.-K.; Kim, H. N.; Moon, S. H.; Suh, K. Y. *Proc. Natl. Acad. Sci. U.S.A.* **2009**, *106*, 5639−5644.
(24) Lee, H.; Bhushan, B. *J. Colloid Interface Sci.* **2012**, *372*, 231−238.
(25) Zhao, Y.; Tong, T.; Delzeit, L.; Kashani, A.; Meyyappan, M.; Majumdar, A. *J. Vac. Sci. Technol. B* **2006**, *24*, 331−335.
(26) Kim, Y.; Claus, R. K.; Limanto, F.; Fearing, R. S.; Maboudian, R. *Langmuir* **2013**, *29*, 8395−8401.
(27) Gillies, A. G.; Puthoff, J.; Cohen, M. J.; Autumn, K.; Fearing, R. S. *ACS Appl. Mater. Interfaces* **2013**, *5*, 6081−6088.
(28) Murphy, M. P.; Aksak, B.; Sitti, M. *Small* **2009**, *5*, 170−175.
(29) Autumn, K.; Majidi, C.; Groff, R. E.; Dittmore, A.; Fearing, R. S. *J. Exp. Biol.* **2006**, *209*, 3558−3568.
(30) Kim, S.; Sitti, M. *Appl. Phys. Lett.* **2006**, *89*, 261911.
(31) del Campo, A.; Greiner, C.; Álvarez, I.; Artz, E. *Adv. Mater.* **2007**, *19*, 1973−1977.
(32) del Campo, A.; Greiner, C.; Arzt, E. *Langmuir* **2007**, *23*, 10235−10243.
(33) Gorb, S.; Varenberg, M.; Peressadko, A.; Tuma, J. *J. R. Soc., Interface* **2007**, *4*, 271−275.
(34) Kwak, M. K.; Jeong, H. E.; Bae, W.-G.; Jung, H.-S.; Suh, K. Y. *Small* **2011**, *7*, 2266−2300.
(35) Schubert, B.; Lee, J.; Majidi, C.; Fearing, R. S. *J. R. Soc., Interface* **2008**, *5*, 845−853.
(36) Abusomwan, U.; Sitti, M. *Appl. Phys. Lett.* **2012**, *101*, 211907.
(37) Gravish, N.; Wilkinson, M.; Autumn, K. *J. R. Soc., Interface* **2008**, *5*, 339−348.
(38) Xia, Y. N.; Whitesides, G. M. *Annu. Rev. Mater. Sci.* **1998**, *28*, 153−184.